Medical Engineering and Physics 115 (2023) 103979

Contents lists available at ScienceDirect

Medical Engineering and Physics

journal homepage: www.elsevier.com/locate/medengphy

A hybrid orthosis combining functional electrical stimulation and soft robotics for improved assistance of drop-foot

Lucy Hodgins *, Chris T. Freeman

School of Electronics and Computer Science, Faculty of Engineering and Physical Sciences, University of Southampton, Southampton, SO17 1BJ, Hampshire, United Kingdom

ARTICLE INFO

Keywords:
Drop foot
Soft robotics
Electrical stimulation
Feedback control
Assistive technology
Hybrid orthosis

ABSTRACT

Drop-foot is characterised by an inability to lift the foot, and affects an estimated 3 million people worldwide. Current treatment methods include rigid splints, electromechanical systems, and functional electrical stimulation (FES). However, these all have limitations, with electromechanical systems being bulky and FES leading to muscle fatigue.

This paper addresses the limitations with current treatments by developing a novel orthosis combining FES with a pneumatic artificial muscle (PAM). It is the first system to combine FES and soft robotics for application to the lower limb, as well as the first to employ a model of their interaction within the control scheme. The system embeds a hybrid controller based on model predictive control (MPC), which combines FES and PAM components to optimally balance gait cycle tracking, fatigue reduction and pressure demands. Model parameters are found using a clinically feasible model identification procedure. Experimental evaluation using the system with three healthy subjects demonstrated a reduction in fatigue compared with the case of only using FES, which is supported by numerical simulation results.

1. Introduction

Drop-foot is a condition affecting approximately 3 million people worldwide [1]. It is often caused by neurological injury and is primarily associated with an inability to control the tibialis anterior (TA) muscle. This leads to reduced dorsiflexion, causing the foot to hang down during the swing phase of the gait cycle [2]. The result is then an abnormal gait pattern, and an increased risk of falls and injury [3].

The most common treatments for drop-foot are ankle-foot orthoses (AFOs) and functional electrical stimulation (FES), with one study citing 47% of patients and carers having used FES and 37% having used a rigid AFO in their rehabilitation [4].

FES involves applying electrical impulses to the peroneal nerve, leading to artificial contraction of the TA muscle. Simple triggered FES systems are employed commercially [5], but a variety of studies have developed more advanced control methods and automated electrode configuration [6–8]. FES has demonstrated improved orthotic effect when compared to AFOs in relation to obstacle avoidance [9], as well as a long-term increase in the volitional activity of the TA muscle [10]. However, prolonged use of FES leads to muscle fatigue, resulting in physical discomfort and a reduction in muscle force output [11].

The most basic AFOs consist of a rigid splint that either limits plantar flexion or provides torque to assist dorsiflexion [9]. These have been shown to improve short-term balance and walking ability [12], and there has been significant research into integrating active elements such as motors, hydraulics, and elastic actuators [13,14]. These active ankle-foot orthoses (AAFOs) have demonstrated success in assisting drop-foot [15] but their wide-spread use is limited by their bulkiness, lack of portability, and difficulties with ensuring correct joint alignment [16].

An alternative to the above rigid AFOs is to use soft robotics, making use of compliant materials to engineer lighter, safer, and more comfortable devices. One example is the treatment of drop-foot in children using pneumatic artificial muscles (PAMs) [17], which are inexpensive, easy to make actuators whose length can be altered by varying their internal pressure. However, their performance has been limited in terms of their speed of actuation, and the relatively high torque requirements mean that a large external compressor is often required. Furthermore, depending on the method of attachment, actuation can lead to strap movement, reducing the assistive torque.

In recent years, research has focused on treating drop-foot using a combination of FES and electromechanical AFOs to decrease the required stimulation intensity and thus reduce the fatigue experienced

* Corresponding author.
E-mail address: lgh1g19@soton.ac.uk (L. Hodgins).

https://doi.org/10.1016/j.medengphy.2023.103979
Received 14 September 2022; Received in revised form 16 March 2023; Accepted 6 April 2023
Available online 11 April 2023

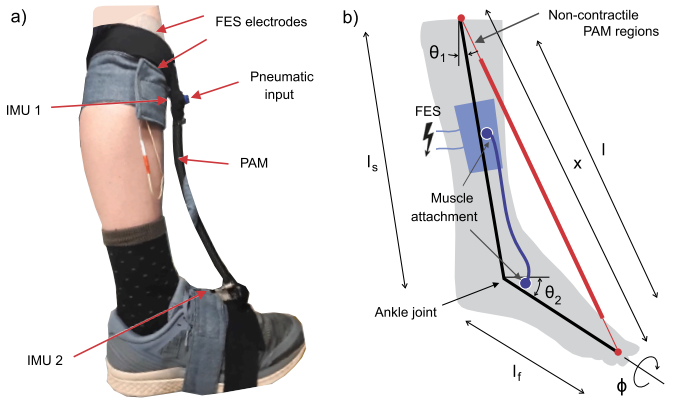

Fig. 1. a) Attachment of the FES electrodes, IMUs, and PAM to the lower leg and foot, with b) corresponding sagittal plane geometry where ankle dorsiflexion is $\theta = \theta_1 + \theta_2$ and eversion/inversion is ϕ.

[18,19]. This hybrid approach also reduces the AFO torque requirement, allowing for smaller, more compact devices. However, current systems still have the same limitations as purely electromechanical AFOs, the most notable being that they are uncomfortable and bulky. Whilst devices have been created that combine soft robotics and FES for hand rehabilitation, so far none have been designed for the treatment of drop-foot, or for lower limb rehabilitation more generally. A further challenge is how to control hybrid AFOs. Few hybrid control approaches have been applied to drop-foot, and previous approaches typically involved switching between control using FES and an AAFO [18], which does not fully utilise the benefits of the hybrid system (i.e. maintaining gait while ensuring hybrid components minimise FES-induced fatigue and AAFO size).

Another hybrid approach applied electromechanical support and FES to different joints [20]. This also failed to capitalise on the potential benefits of a hybrid system, and was more applicable to treating multiple gait abnormalities rather than purely drop-foot. Model-predictive control was applied to a hybrid system where it enabled patients with spinal cord injury to maintain a desired knee angle [21]. However it has not yet been used in the treatment of drop-foot.

This paper provides the following novel contributions. It develops the first hybrid ankle-foot orthosis to combine FES with soft robotics. A PAM is selected to reduce FES-induced muscle fatigue whilst improving comfort compared to more traditional AAFOs. The paper then develops an integrated FES and PAM dynamic model, together with a comprehensive identification scheme suitable for clinical deployment. An optimal control approach is also developed to allow FES and the PAM to be actuated simultaneously, in contrast to previous approaches used to treat drop-foot. This enables tracking performance and fatigue reduction to be balanced for the first time. A prototype system is then created and tested on three healthy individuals to evaluate the model and examine the control performance with respect to both gait cycle tracking and fatigue reduction.

2. Device design

Fig. 1 shows the proposed hybrid device. The ankle is actuated by the combined torque generated by FES stimulation (due to surface electrodes placed over the TA muscle and peroneal nerve) and PAM contraction. The PAM is anchored at one end to the lower leg, with the other end attaching to the foot. Fabric straps ensure increased user comfort compared to the rigid systems used in [18] and [19].

The PAM is manufactured from latex rubber tubing covered in a polyester braided sheath. Pressure is controlled using two solenoid valves (Adafruit industries, 1/2″, 12 V) driven by a compressor (Clarke tools, UK) which provides a maximum pressure of 800 kPa. Inertial measurement units (IMUs) (MPU6050) attached to the knee and foot

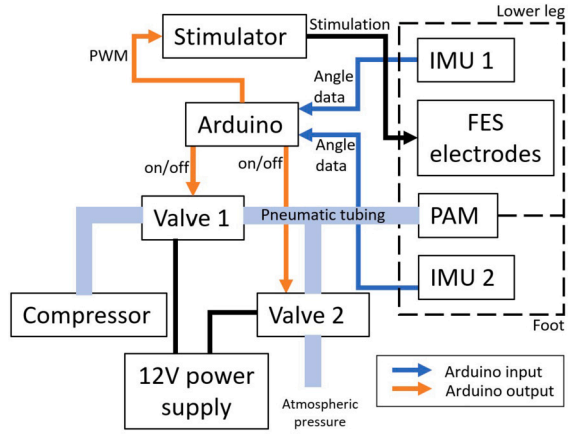

Fig. 2. Schematic showing hardware components.

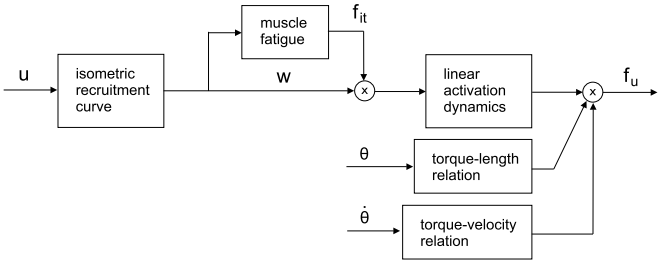

Fig. 3. Block diagram showing force f_u generated by electrically stimulated TA muscle.

transmit data to a microcontroller (Arduino Uno SMD). These embed Kalman filters and provide angles θ, ϕ (accuracy ±1.8°). FES stimulation is applied using a biphasic stimulator (Odstock Medical Ltd, UK) and controlled using pulse-width modulation (PWM), with the pulsewidth varied between 0-300 μs at a frequency of 40 Hz. These components are shown in Fig. 2 and will be subsequently discussed.

2.1. Modelling

The parameter selection and control strategy are based on a dynamic model of the hybrid system, which will be constructed by selecting and combining models of the individual components, as described next.

2.1.1. Muscle model

Human muscle has been modelled in a variety of different ways [22–26], but the most common form is a Hammerstein structure comprising a static non-linear isometric recruitment curve (IRC) in series with the muscle's linear activation dynamics (LAD). The IRC relates the input stimulation signal $u(t)$ to the muscle activation, and is denoted $h_{IRC}(u)$. The LAD relates the muscle activation to muscle output force, and is denoted by transfer function $G(s)$. The output is then multiplied by force-length and force-velocity relationships $f_{FL}(\theta)$ and $f_{FV}(\dot{\theta})$ to produce the overall force. Passive muscle properties will be added in Section 2.1.3.

There are a variety of models representing FES-induced muscle fatigue [27–29], but one of the simplest was proposed by [30] and involves multiplying the output w of the IRC by a time-varying term, $f_{it}(t)$ that satisfies

$$\frac{df_{it}(t)}{dt} = \frac{(f_{min} - f_{it}(t))\lambda w(t)}{\tau_{fat}} - \frac{(1 - f_{it}(t))(1 - \lambda w(t))}{\tau_{rec}} \quad (1)$$

where f_{min} is the minimum fitness, λ is a scaling factor dependant on stimulation frequency, and τ_{fat} and τ_{rec} are the time constants for muscle fatigue and recovery respectively. The resulting overall muscle dynamics are shown in Fig. 3.

2.1.2. PAM and valve modelling

The static force produced by a PAM is commonly given by

$$f_{static}(\epsilon, p) = \pi r_0^2 p \left(\frac{3(1-k\epsilon)^2}{\tan^2(\alpha_0)} - \frac{1}{\sin^2(\alpha_0)} \right) \tag{2}$$

where p is the pressure, r_0 is the initial PAM radius, α_0 is the initial braid angle, and ϵ is the strain, equal to the ratio of PAM extension to its initial length. From the geometry in Fig. 1, the latter is equal to

$$\epsilon = \frac{\sqrt{l_s^2 + l_f^2 - 2l_f l_s \sin(\theta_0)} - \sqrt{l_s^2 + l_f^2 - 2l_f l_s \sin(\theta)}}{l_0} \tag{3}$$

where θ_0 is the ankle angle when the PAM is relaxed, with l_0 later denoting the corresponding PAM length. The experimentally-derived parameter k accounts for the non-cylindrical nature of the device [31]. Relation (2) will be used in Section 4 to optimise PAM parameters, ensuring suitable force and pressure properties over the required contraction range.

There are a variety of dynamic models of PAM behaviour [32,33], and a common form is obtained by adapting the above static model to include the effects of friction and surface contact forces [31] to give

$$f_p = f_{static} - f_{fric}(1/n) S_{contact} p \operatorname{sgn}(\dot{z}) \tag{4}$$

where $z = \epsilon l_0$ is the PAM displacement, $1/n$ is the proportion of the muscle surface rubbing against itself, $S_{contact}$ is the thread contact surface area given by

$$S_{contact} = 2\pi r_0 l_0 \frac{\sin(\alpha_0)}{(1-k\epsilon)\sqrt{1-\cos^2(\alpha_0)(1-k\epsilon)^2}} \tag{5}$$

and f_{fric} is the dynamic friction coefficient given by

$$f_{fric} = f_k + (f_s - f_k)\exp(\dot{z}/\dot{z}_s) \tag{6}$$

where f_s and f_k are the static and kinetic friction coefficients respectively, and $\dot{z}_s$ is a velocity constant.

While it is possible to control PAM pressure using servo valves, as done in [34], a commonly applied approach uses PWM control of on/off solenoid valves [35,36]. This reduces cost and control complexity. In both cases, PAM pressure is related to the mass flow $\dot{m}$ through the valve by

$$\dot{p} = \frac{kRT}{v_p(z)} \dot{m}(u_v, p) - pk \frac{\dot{v}_p(z)}{v_p(z)} \tag{7}$$

where again $z = \epsilon l_0$, k, R, T, v_p are the specific heat ratio, gas constant, temperature, and PAM volume respectively, and u_v is the duty cycle of the valve. It is shown in [35] that a static linear relationship can accurately capture $v_p(z)$.

For the fastest PAM response, each valve shown in Fig. 2 must be energised while the other is de-energised. Defining u_{v1} and u_{v2} as the duty cycles of valves 1 and 2 respectively, the combined state is $u_v = (u_{v1}, u_{v2})$. While it is then possible to model $\dot{m}(u_v, p)$ using standard flow-rate equations, in cases where the duty cycle is high (i.e. rapid switching) this relationship is typically determined experimentally. A quadratic form validated in [37] is

$$\begin{aligned} \dot{m}(u_v, p) = &\sqrt{(p_c - p)}(m_1 u_{v1} + m_2 u_{v1}^2) \\ &- (p_a - p)(m_3 u_{v2} + m_4 u_{v2}^2) \end{aligned} \tag{8}$$

where p_a and p_c are atmospheric pressure and the pressure of the compressor respectively, and m_{1-4} are experimentally-derived coefficients. A bi-polynomial form was proposed in [38] but contains more parameters.

The overall muscle and valve dynamics are shown in Fig. 4.

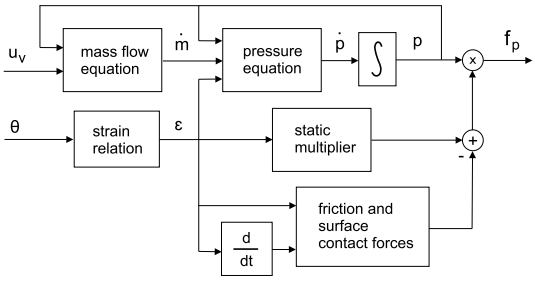

Fig. 4. Block diagram showing force f_p generated by PAM valve state u_v.

2.1.3. Rigid body dynamics

The FES and the PAM torques actuate the ankle joint, which can be modelled by the general relationship

$$\begin{aligned} M_u(q) f_u + M_p(q) f_p = &B(q)\ddot{q} + C(q,\dot{q})\dot{q} + F_s \operatorname{sgn}(\dot{q}) + \\ &F_d(q,\dot{q}) + g(q) + g_{FL}(q) + g_{FV}(\dot{q}) - J(q)h \end{aligned} \tag{9}$$

where joint vector $q = [\theta, \phi]^\top$, h is a vector of externally applied forces and torques, and $J(q)$ is the system Jacobian. Matrices $B(q)$ and $C(q,\dot{q})$ are the inertial and Coriolis matrices respectively, $F_d(q,\dot{q})$ is dynamic friction, $F_s \operatorname{sgn}(q)$ is the static friction, $g(q)$ comprises gravity and contact forces, and $g_{FL}(q)$ and $g_{FV}(\dot{q})$ represent the muscle elasticity and viscosity respectively. Vectors $M_u(q)$ and $M_p(q)$ are the moment arms of the TA muscle and PAM respectively. Functional forms appear in, e.g. [39,40].

The component of $M_p(q)$ about the θ axis is

$$l_s \sin\left(\operatorname{acos}\left(\frac{l_s^2 + x(\theta)^2 - l_f^2}{2 l_s x(\theta)} \right) \right) = \sqrt{l_s^2 - \left(\frac{l_s^2 + x(\theta)^2 - l_f^2}{2x(\theta)} \right)^2} \tag{10}$$

where

$$x(\theta) = \sqrt{l_s^2 + l_f^2 + 2 l_s l_f \sin\theta}. \tag{11}$$

The muscle moment arm, $M_u(q)$, is typically assumed constant [25]. It is widely assumed in the literature that the PAM acts only in a single plane and that FES pads are positioned to minimise eversion/inversion. In this case $q = \theta$ may be assumed.

3. Identification and control

The hybrid system combines components (2)-(11) and is shown in Fig. 5 where

$$\begin{aligned} g(q,\dot{q}) = &J(q)h - C(q,\dot{q})\dot{q} - F_s \operatorname{sgn}(\dot{q}) - F_d(q,\dot{q}) \\ &- g(q) - g_{FL}(q) - g_{FV}(\dot{q}) \end{aligned} \tag{12}$$

$$\begin{aligned} f(q) = &M_p(q)\left(\pi r_0^2 \left(\frac{3(1-k\epsilon)^2}{\tan^2(\alpha_0)} - \frac{1}{\sin^2(\alpha_0)} \right) \right. \\ &\left. - f_{fric}(1/n) S_{contact} \operatorname{sgn}(z) \right) \end{aligned} \tag{13}$$

$$h(q,\dot{q}) = M_u(q) f_{FL}(\theta) f_{FV}(\dot{\theta}) \tag{14}$$

$$\begin{aligned} d(u_v, p, q) = &\frac{kRT}{v_p(l_0\epsilon)} \left(\sqrt{(p_c - p)}(m_1 u_{v1} + m_2 u_{v1}^2) - \right. \\ &\left. (p_a - p)(m_3 u_{v2} + m_4 u_{v2}^2) \right) - pk \frac{\dot{v}_p(l_0\epsilon)}{v_p(l_0\epsilon)} \end{aligned} \tag{15}$$

$$y(w, w_f) = \left(\frac{(f_{min} - \frac{w_f}{w})\lambda w}{\tau_{fat}} - \frac{(1 - \frac{w_f}{w})(1 - \lambda w)}{\tau_{rec}} \right) \tag{16}$$

System parameters can be identified by extending the identification procedure of [40] for an FES actuated upper limb. The resulting procedure comprises the following seven experimental tests.

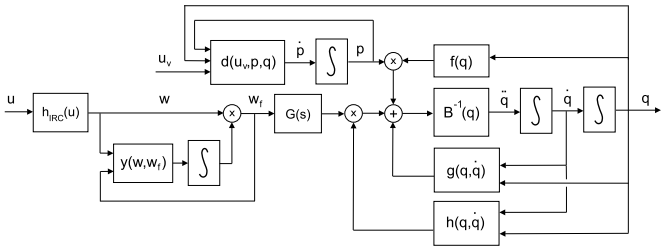

Fig. 5. Complete hybrid FES/PAM ankle system dynamics.

Definition 1 *(Identification Procedure)*. Consider the system shown in Fig. 5 with components (3), (12)-(16). Let an external force/torque vector h be applied to the participant's foot (e.g. by attaching a six axis sensor to the shoe and manipulating a handle attached to the sensor). Then the model components can be identified using the following procedure:

1. Apply force/torque to move the foot through a prescribed angular motion, with no FES or valve input ($u = u_v = 0$). Measure h and q at sample times $\mathcal{T} = \{0, \Delta T, \cdots, T\}$ and denote the data set as $\{h(t), q(t)\}_{t\in\mathcal{T}}$. Determine rigid body components $B(q)$ and $g(q, \dot{q})$ via least-squares fitting as described in [40].
2. Apply external force/torque to fix foot at angle $q = 0$. Apply FES ramp signal $u(t)$ and record data $\{u(t), h(t)\}_{t\in\mathcal{T}}$. Compute FES components $h_{IRC}(u)$ and $G(s)$ via least-squares fitting, as described in [40].
3. Apply force/torque to fix foot at angle $q = 0$. Apply FES signals described in [41] and record data set $\{u(t), h(t)\}_{t\in\mathcal{T}}$. Compute $\{w(t), w_f(t)\}_{t\in\mathcal{T}}$ using known $h_{IRC}(u)$ and $G(s)$, and apply nonlinear minimisation to fit parameters λ, f_{min}, τ_{fat}, τ_{rec} such that $y(w, w_f)w = w_f$.
4. Apply force/torque to move foot through prescribed motion while also applying fixed FES level $u > 0$. Fit active FES function $h(q, \dot{q})$ to measured data set $\{h(t), q(t), u(t)\}_{t\in\mathcal{T}}$ using $f_{FL}(\theta)$, $f_{FV}(\dot{\theta})$ parameterisations given in [40].
5. Repeat test (4) substituting fixed FES level by fixed valve PAM input. Fit PAM function $f(q)$ parameters to measured data set $\{h(t), q(t), p(t)\}_{t\in\mathcal{T}}$.
6. Attach PAM directly to a compressor and vary internal pressure p, whilst recording $\{v_p(t), z(t)\}_{t\in\mathcal{T}}$. Assume the linear $v_p(z(t))$ form given in [35] and fit parameters via least-squares.
7. Connect valves as shown in Fig. 2, without attaching device to participant, then set $u_{v2} = 0$ and record $\{\dot{m}(t), p(t)\}_{t\in\mathcal{T}}$ for varying u_{v1}. Following this, inflate PAM to maximum pressure, set $u_{v1} = 0$, and record $\{\dot{m}(t), p(t)\}_{t\in\mathcal{T}}$ for varying u_{v1}. Determine $\dot{m}(u_v(t), p(t))$ using least-squares fitting, taking form (8). This then yields $d(u_v, p, q)$ since $v_p(z(t))$ is known and k, R, and T are constant.

Tests (6)-(7) are independent of the participant and only need to be performed once.

3.1. Control objective

The objective for people with drop-foot is to track the swing phase of the gait cycle, $t \in [t_{swing}, T]$ shown in Fig. 6. This motivates computing the signals $u(t)$, $u_v(t)$, $t \in [0, T]$ that solve the minimisation problem

$$\arg\min J(u, u_v), \tag{17}$$

$$J(u, u_v) := \int_{t_{swing}}^{T} (\theta_{ref}(\tau) - \theta(\tau))^2 d\tau + w_1 \int_0^T (1 - fit(\tau))^2 d\tau + w_2 \int_0^T p(\tau)^2 d\tau$$

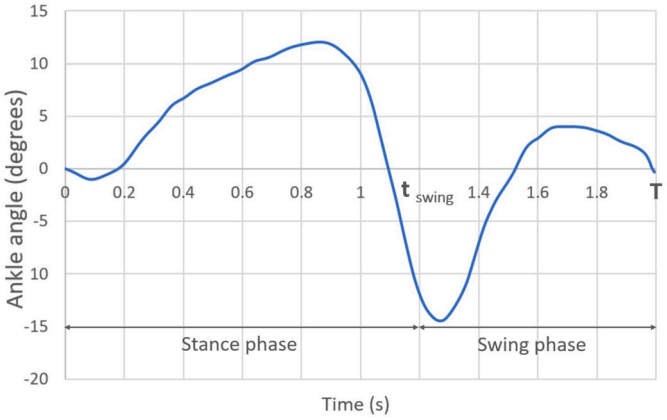

Fig. 6. Changes in ankle angle over time for a typical gait cycle, based on data collected in [42].

subject to dynamics (3), (12)-(16) and constraints

$$0 < p(t) < 600, \quad t \in [0, T]$$
$$0 < u(t) < 300, \quad t \in [0, T] \tag{18}$$

where positive-definite weights w_1 and w_2 are used to affect a compromise between reducing FES-induced fatigue and limiting the effort required from the PAM.

To make the computation tractable using embedded hardware, MPC is selected due to its previous success for constrained hybrid systems. At every time instant t_k, MPC solves (17) over a receding horizon of length t_m, i.e. the time interval $t \in (t_k, t_k + t_m]$. The minimisation problem therefore becomes

$$\arg\min J(\bar{u}, \bar{u}_v), \tag{19}$$

$$J(\bar{u}, \bar{u}_v) := \int_{\max\{t_k, t_{swing}\}}^{\max\{t_k+t_m, t_{swing}\}} (\theta_{ref}(\tau) - \theta(\tau))^2 d\tau + w_1 \int_{t_k}^{t_k+t_m} (1 - fit(\tau))^2 d\tau + w_2 \int_{t_k}^{t_k+t_m} p(\tau)^2 d\tau$$

where $\bar{u} = (u(t_k), u(t_k + t_m)]$ and $\bar{u}_v = (u_v(t_k), u_v(t_k + t_m)]$ are the inputs over the receding horizon. Minimisation (19) is solved by applying a suitable constrained nonlinear optimization algorithm to dynamics (12)-(16) and constraints (18), starting from time $t = t_k$. Many software programs exist, e.g. SNOPT, FilterSQP, Ipopt, Knitro, Lancelot. Having computed the optimal inputs $\bar{u}^*$, $\bar{u}_v^*$, only the first element of each is then applied to the physical system. The computation is then repeated for the next time instant.

Remark 2. The MPC solution of (19) has a feedback structure as it depends on the current system state, and converges to the global solution of (17) as the predictive horizon $t_m \to T$.

3.2. Implementation

Solving minimisation (17) can be simplified by imposing additional structure on the form of u and u_v. An obvious choice is to specify that u is the output of a PID controller that is fed by the tracking error, since this is a common choice of FES schemes and requires only three parameters (PID gains k_p, k_i, and k_d). Additionally limiting FES to only be applied for the first 0.5 s of swing phase can be shown to maximise performance in experimental trials, since beyond this point the cost of fatigue has been found to outweigh improvements in tracking performance.

Signal u_v can also be simplified by specifying that the PAM is only inflated and deflated once per gait cycle. This method of control is sim-

ilar to that used in [43], and requires only two parameters (contraction time t_{pr}, and relaxation time t_{pc}). These forms are then substituted into optimisation (17) which simplifies to

$$\arg\min J(k_p, k_i, k_d, t_{pr}, t_{pc}), \tag{20}$$

$$J(k_p, k_i, k_d, t_{pr}, t_{pc}) := \int_{t_{swing}}^{T} (\theta_{ref}(\tau) - \theta(\tau))^2 d\tau +$$

$$w_1 \int_0^T (1 - fit(\tau))^2 d\tau + w_2 \int_0^T p(\tau)^2 d\tau$$

subject to the original constraints (18) and the additional constraints

$$u_v(t) = \begin{cases} (0,1), & 0 \le t < t_{pc} \\ (1,0), & t_{pc} \le t < t_{pr} \\ (0,1), & t_{pr} \le t < T \end{cases}$$

$$u(t) = \begin{cases} u, & 0 \le t \le (t_{swing} + 0.5) \\ 0, & t > (t_{swing} + 0.5) \end{cases} \tag{21}$$

Since the minimisation requires only five parameters, it is possible to perform on small, low-cost hardware.

4. Experimental design and results

Following ethics approval (FEPS\ERGO\70971), tests were carried out at the University of Southampton on three healthy adults between the ages of 20-23, in order to test the feasibility of the system.

4.1. Model components

The PAM length l_0 and radius r_0 were calculated to satisfy $-15 < \theta < 5$ for $0 < p < 600$, in accordance with (2). This produced PAM dimensions of 9 mm diameter and 30 cm length.

4.2. Model identification

The procedure in Definition 1 was applied with the following signal and functional forms chosen to minimise testing duration and resources.

In step (1) the rigid body dynamics components $B(q)$ and $g(q, \dot{q})$ were chosen as described in [44]. In step (2) $u(t)$ was selected as a slow ramp when determining $h_{IRC}(u)$, and $G(s)$ took the form given in [45,25]. For ease of measurement θ was recorded in place of h. Step (3) was replaced by instead using parameter values estimated using data from [46] in order to minimise muscle fatigue. Likewise in step (4) the functions $f_{FL}(\theta)$, $f_{FV}(\dot{\theta})$ were omitted since the angular range and velocity during a typical gait cycle produces negligible effect.

For step (5) $h(t)$ was generated using model components previously described and a measured data set $\{q(t), p(t)\}$. In step (7) the simplified valve constraints (21) meant that the valve function $d(u_v, p, q)$ could be expressed by $d(t_{pc}, t_{pr})$, and the valve function could then be determined experimentally by measuring $p(t)$ for $u_v = (1,0)$, $p(0) = p_a$ and $u_v = (0,1)$, $p(0) = p_c$.

Table 1 gives the identification procedure fitting and prediction accuracy for the complete system shown in Fig. 5 with $u_v(t) = 0$. Accuracies are stated as a percentage in accordance with

$$Accuracy = 100\left(1 - \frac{\|\theta - \hat{\theta}\|_2}{\|\theta - \overline{\theta}\|_2}\right) \tag{22}$$

where θ is the measured ankle angle, $\hat{\theta}$ is the angle recorded by the model, and $\overline{\theta}$ is the mean of θ.

Prediction results were obtained by splitting the data collected over a number of trials in two, with the model being fitted to one half of these before being used to predict the outcome of the other half.

Table 1
Fitting and prediction accuracy of full model with $u_v(t) = 0$.

Experiment no	Fitting accuracy (%)	Prediction accuracy (%)
1	48.3	44.0
2	79.3	77.9
3	56.3	46.8

Table 2
Fitting and prediction accuracy for the IRC curves.

Experiment no	Fitting accuracy (%)	Prediction accuracy (%)
1	85.7	83.2
2	88.9	83.9
3	85.3	74.8

Table 3
Optimal simulation parameter values.

	k_p	k_i	k_d	t_{pc}	t_{pr}
Hybrid	10	5	500	0.06	0.69
PAM	N/A	N/A	N/A	0.03	0.74
FES	1000	5	100	N/A	N/A

Table 4
Values of cost function (20) for FES simulation.

k_p	k_d		
	10	100	500
10	870.4	621.8	620.1
100	679.6	624.9	626.4
500	947.1	650.8	628.3
1000	1064.8	812.7	651.9

Average fitting and prediction accuracies of 61.3% and 56.2% were obtained for the full model. Results were also calculated for identification of the parameters of $h_{IRC}(u)$, as given in Table 2. These were significantly higher than for the full model, with average fitting and prediction accuracies of 86.6% and 80.6% respectively.

4.3. Numerical validation

Optimisation weights w_1 and w_2 were selected as 5.4×10^4 and 1.35×10^{-3} respectively to ensure comparable contribution of pressure and fatigue terms within the cost function. Using these weights the control cost (20) was minimised using values given in Table 3, corresponding to a cost of $J = 606$. This resulted in a tracking accuracy of 98.7%, calculated using

$$Accuracy = 100\left(1 - \frac{\|\theta_{out} - \theta_{ref}\|_2}{\|\theta_{out} - \theta_{base}\|_2}\right) \tag{23}$$

where θ_{out} is the output angle of the model, θ_{ref} is the reference signal being tracked, and θ_{base} is a baseline angle used to normalise the error. This baseline was set equal to the ankle angle at the beginning of the swing phase of the gait cycle.

To investigate sensitivity, Table 4 gives the cost function for varying values of parameters k_p and k_d. The integral gain k_i was fixed at 5, and variation in this parameter resulted in little change in the cost function.

Table 5 gives the value of the cost function for four different values of t_{pc} and t_{pr}. The optimal tracking for the hybrid system is shown in Fig. 7, along with the output angle when using purely FES and purely the PAM. This reveals significantly better performance (lower cost function) when combining FES and the PAM than when they were applied individually.

Table 5
Values of cost function (20) for PAM simulation.

$t_{pc}(s)$	$t_{pr}(s)$			
	0.2	0.4	0.6	0.8
0	2253	1095	854	963
0.2	1815	1422	1018	930
0.4	N/A	1815	1523	1637
0.6	N/A	N/A	1815	1738

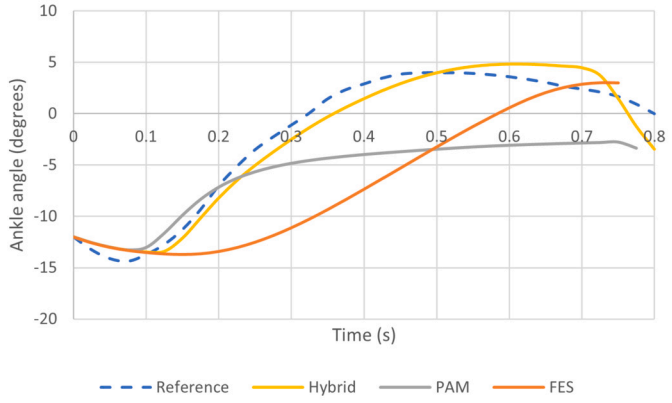

Fig. 7. Tracking when using purely FES, purely the PAM, and the hybrid system with parameter values as stated in Table 3.

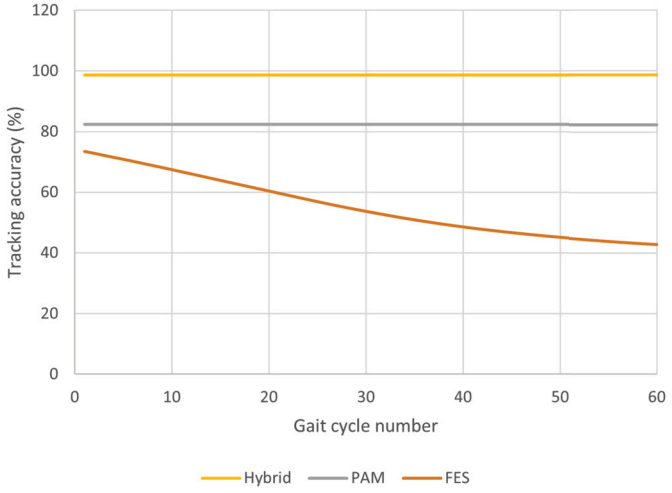

Fig. 8. Comparison of tracking accuracy over subsequent gait cycles when using purely FES, purely the PAM, and with the hybrid system.

Simulations were also used to investigate the long-term tracking ability of the device, as well as the difference in muscle fatigue when using the PAM compared to using purely FES.

Fig. 8 shows the simulated tracking accuracy over the course of 60 gait cycles when using purely FES, purely the PAM, and the hybrid system. The parameter values in Table 3 were again applied. This graph reveals a significant reduction in accuracy over time when using purely FES that is not seen with the hybrid approach. The initial accuracy of the FES-only and PAM-only system is also less.

Defining muscle fatigue as $1 - f_{it}(t)$, simulations revealed a much sharper increase in fatigue when using purely FES compared to the hybrid system, as shown in Fig. 9. Furthermore the point at which muscle fatigue flattened out (i.e. where fatigue during swing phase was balanced by recovery during stance) was greater when using FES compared to the hybrid system (0.51 compared to 0.45).

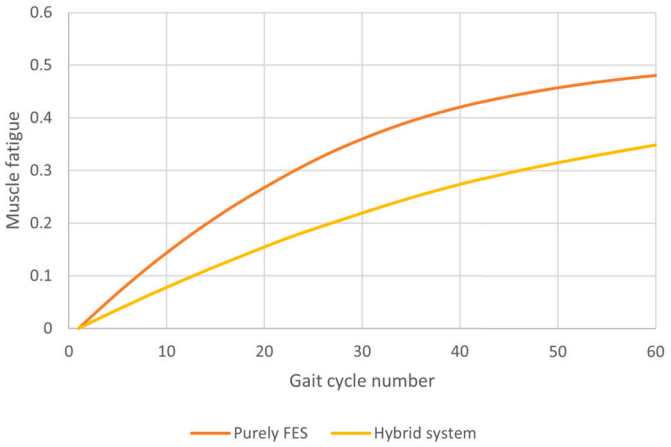

Fig. 9. The progression of fatigue (defined as 1-fitness) over 60 gait cycles when using purely FES compared to the hybrid system.

Table 6
Experimental gait cycle tracking accuracies.

Participant no	FES tracking accuracy (%)	Hybrid system tracking accuracy (%)
1	−22.3	49.4
2	8.47	51.8
3	33.0	81.2

4.4. Experimental gait tracking

Following model identification each participant underwent trials to determine the tracking accuracy when using both purely FES and the hybrid system. Each 'gait cycle' involved applying stimulation such that the participant's ankle tracked the swing phase shown in Fig. 6, followed by a brief pause in which the foot was allowed to drop down towards the natural resting position. At the point at which the ankle reached the threshold angle indicative of the start of the swing phase (defined using data from [42]) the stimulation was applied again. This process was repeated 60 times. Each participant was allowed to rest for 20 minutes between testing the FES and hybrid systems to allow for muscle recovery.

Table 6 compares the % tracking accuracy of the FES and hybrid system averaged over 60 gait cycles for each trial. This reveals a poor tracking accuracy of only 6.4% when using purely FES, compared with a much greater accuracy of 60.8% when using the hybrid system.

Fig. 10 shows representative results for the gait cycle tracking accuracy over the course of 60 gait cycles when using purely FES, alongside that when using the hybrid system. The general trend reveals a decrease in tracking ability when using FES which contrasts with the hybrid system, for which tracking accuracy remains fairly constant. This is consistent with the simulation results given in Fig. 8.

4.5. Experimental fatigue results

In order to measure changes in muscle fatigue, a stimulation pulse of 300 μs intensity and 1 s duration was applied at the start and end of both gait cycle tracking experiments. The muscle response to the first pulse acted as a baseline for initial muscle fitness, which was then compared to the response to the final pulse in order to quantify fatigue.

Table 7 shows the changes in ankle angle, $\Delta\theta$, in response to the 300 μs stimulation input before and after the gait cycle tracking experiments for both the FES and hybrid system. In all cases a significantly smaller muscle response was observed after 60 gait cycles using FES compared to before, but this same decrease was not seen when using the hybrid system.

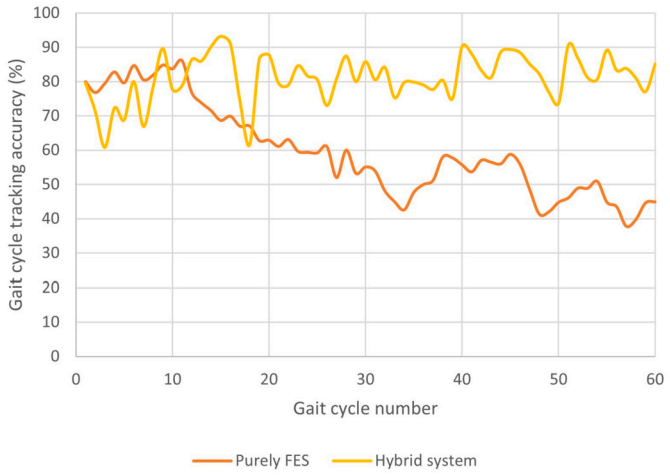

Fig. 10. Comparison between the experimental tracking accuracy for participant 3 when using purely FES compared to the hybrid system.

Table 7
Change in muscle response (°) due to stimulation for purely FES and hybrid control, pre and post gait tracking.

Experiment	FES		Hybrid	
	$\Delta\theta$ pre	$\Delta\theta$ post	$\Delta\theta$ pre	$\Delta\theta$ post
1	17.4	2.18	9.9	9.85
2	33.91	9.57	14.16	35.9
3	29.02	18.83	22.2	30.95

5. Discussion

The motivation behind the hybrid approach proposed in this paper was to reduce the disadvantages associated with using either purely FES or soft robotics when assisting people with drop-foot. These include FES-induced muscle fatigue and the reduction in performance that can occur due to poor AFO fitting.

A primary benefit of this device is its ability to reduce fatigue when compared to using purely FES. This has been successfully demonstrated in simulation, and experimental results confirm a significant benefit. Furthermore, the hybrid device demonstrates a clear improvement over using purely FES when considering long-term tracking accuracy, as shown in Figs. 8 and 10. Another advantage of the hybrid approach is the increased gait tracking accuracy observed both in simulation and experimental results when compared to using either FES or the PAM individually.

In terms of the usability of the system, there are still some challenges that need to be overcome. Studies have revealed that the most important features of an assistive device to impact on user experience are comfort and ease of setup/use [4], properties that are limited in the proposed system by the need for a compressor to actuate the PAM. While the current setup requires the user to be tethered to an external compressor, a number of similar soft robotic systems have succeeded in attaching a light-weight compressor to the trunk of the body [47,48]. This positioning allows for total portability whilst reducing the mass of the system at the extremities, increasing user comfort. It is therefore a potential solution. The total weight of the proposed ankle-foot orthosis is 102 g, significantly less than similar pneumatic AFOs, e.g. [43,49,50]. With regards to ease of setup, successful FES stimulation currently requires correct positioning of the electrodes, which may be difficult for users to achieve. Furthermore, the requirement to carry out the identification procedure in Definition 1 significantly increases setup time. These issues are addressed in the next section.

A secondary aim of this paper, alongside the fabrication of a physical device, was to present a model that could be used to predict optimal control parameter values. The proposed model and identification procedure was unique in its ability to combine both FES and soft robotics. It also accounted for the occurrence of muscle fatigue, a factor which is often ignored when identifying muscle dynamics in similar papers (e.g. [51]). The model of FES muscle response was found to have relatively high fitting and prediction accuracy when compared with similar FES identification papers (e.g. [52]). The control approach was presented as a general minimisation problem, enabling the designer to choose either an MPC solution form, or to impose additional constraints that simplify the computation and allow solutions to be implemented on low cost, portable hardware.

6. Conclusions and future work

This paper is the first to demonstrate the feasibility of combining FES and soft robotics for the treatment of drop-foot. A device was created combining a PAM with FES, with all three experiments demonstrating a significant decrease in the fatigue experienced when using the hybrid system compared to purely FES. This paper has also presented a novel simulation used to predict optimal parameters for hybrid control. This further revealed the benefit of the system in terms of minimising muscle fatigue and maximising tracking accuracy.

Future work focuses primarily on further improving the tracking ability of the experimental system by implementing a more advanced control approach, before increasing the number of participants the device is tested on. Additionally, the results when testing on persons with drop-foot may be different to those seen for healthy individuals, so following this the system will be validated with a suitable sample of the former group. A questionnaire will also capture user perceptions of the system to inform further development.

Furthermore, if the device were to be used for rehabilitation outside of a clinical environment the size of the hardware would need to be reduced, using a smaller compressor and valve setup and miniaturising the electronics. An electrode array could be used to reduce the need for accurate electrode positioning, and multiple model switched adaptive control (MMSAC) used to reduce identification time. MMSAC works by defining a set of possible model parameters that might represent the true system. It then implements a bank of estimators that compute which model most accurately fits the measured data, and applies the controller designed for the corresponding model. Initial feasibility of combining MMSAC and electrode arrays was established in [53].

Funding

None received.

Ethical approval

Experimental trials were carried out following approval from University of Southampton Ethics Committee (FEPS\ERGO\70971). All participants gave written informed consent.

Declaration of competing interest

None declared.

References

[1] Barrett CL, Taylor PN. The effects of the odstock drop foot stimulator on perceived quality of life for people with stroke and multiple sclerosis. Neuromodulation 2010;13(1):58–64.
[2] Graham J. Foot drop: explaining the causes, characteristics and treatment. Br J Neurosci Nurs 2010;6(4):168–72. https://doi.org/10.1051/matecconf/20178702031.
[3] Peterson EW, Cho CC, Finlayson ML. Fear of falling and associated activity curtailment among middle aged and older adults with multiple sclerosis. Mult Scler J 2007;13(9):1168–75. https://doi.org/10.1177/1352458507079260.

[4] Hughes A-M, Burridge JH, Demain SH, Ellis-Hill C, Meagher C, Tedesco-Triccas L, et al. Translation of evidence-based assistive technologies into stroke rehabilitation: users' perceptions of the barriers and opportunities. BMC Health Serv Res 2014;14(1). https://doi.org/10.1186/1472-6963-14-124.
[5] York G, Chakrabarty S. A survey on foot drop and functional electrical stimulation. Int J Intell Robot Applic 2019;3:4–10. https://doi.org/10.1007/s41315-019-00088-1.
[6] Page A. Repetitive control and electrode array pattern selection for FES-based drop-foot assistance. Ph.D. thesis. University of Southampton; Sept 2020.
[7] Chen Y-L, Chen S-C, Chen W-L, Hsiao C-C, Kuo T-S, Lai J-S. Neural network and fuzzy control in FES-assisted locomotion for the hemiplegic. J Med Eng Technol 2004;28(1):32–8. https://doi.org/10.1080/03091900310001211523.
[8] Seel T, Werner C, Raisch J, Schauer T. Iterative learning control of a drop foot neuroprosthesis: generating physiological foot motion in paretic gait by automatic feedback control. Control Eng Pract 2016;48:87–97. https://doi.org/10.1016/j.conengprac.2015.11.007.
[9] van Swigchem R, van Duijnhoven H, den Boer J, Geurts AC, Weerdesteyn V. Effect of peroneal electrical stimulation versus an ankle-foot orthosis on obstacle avoidance ability in people with stroke-related foot drop. Phys Ther 2012;92(3):398–406. https://doi.org/10.2522/ptj.20100405.
[10] Kottink A, Hermens H, Nene A, Pt M, Groothuis-Oudshoorn C, IJzerman M. Therapeutic effect of an implantable peroneal nerve stimulator in subjects with chronic stroke and footdrop: a randomized controlled trial. Phys Ther 2008;88:437–48. https://doi.org/10.2522/ptj.20070035.
[11] Wan JJ, Qin Z, Wang PY, Sun Y, Liu X. Muscle fatigue: general understanding and treatment. Exp Mol Med 2017;49(10):384. https://doi.org/10.1038/emm.2017.194.
[12] Tyson SF, Kent RM. Effects of an ankle-foot orthosis on balance and walking after stroke: a systematic review and pooled meta-analysis. Arch Phys Med Rehabil 2013;94(7):1377–85. https://doi.org/10.1016/j.apmr.2012.12.025.
[13] Kim J, Hwang S, Sohn R, Lee Y, Kim Y. Development of an active ankle foot orthosis to prevent foot drop and toe drag in hemiplegic patients: a preliminary study. Appl Bionics Biomech 2011;8(3–4):377–84. https://doi.org/10.3233/ABB-2011-0008.
[14] Kikuchi T, Tanida S, Otsuki K, Yasuda T, Furusho J. Development of third-generation intelligently controllable ankle-foot orthosis with compact mr fluid brake. In: 2010 IEEE international conference on robotics and automation; 2010. p. 2209–14.
[15] Arnez-Paniagua V, Rifâ H, Amirat Y, Mohammed S. Adaptive control of an actuated-ankle-foot-orthosis. In: 2017 international conference on rehabilitation robotics (ICORR); 2017. p. 1584–9.
[16] Dollar AM, Herr H. Lower extremity exoskeletons and active orthoses: challenges and state-of-the-art. IEEE Trans Robot 2008;24(1):144–58. https://doi.org/10.1109/TRO.2008.915453.
[17] Ishak NZ, Mohamaddan S, Kamaruddin AMNA, Khamis H, Yamamoto S, Dawal SZM. Development of ankle foot orthosis (AFO) using pneumatic artificial muscle for disabled children. MATEC Web Conf 2017;87:016007. https://doi.org/10.1051/matecconf/20178702031.
[18] Jung P-G, Huo W, Moon H, Amirat Y, Mohammed S. A novel gait phase detection algorithm for foot drop correction through optimal hybrid FES-orthosis assistance. In: 2021 IEEE international conference on robotics and automation; 2021. p. 10391–7.
[19] Kobravi HR, Farzaneh Y, Faryar Majd M, Sheikh M, Akbarzadeh Tootoonchi A. A human interactive hybrid FES-robotic system applicable to improvement of foot drop after stroke: case report of a patient with chronic stroke. Arch Bone Jt Surg 2020;8(6):744–7. https://doi.org/10.22038/abjs.2020.48595.2410.
[20] Krishnamoorthy V, Hsu W-L, Kesar T, Benoit D, Banala S, Perumal R, et al. Gait training after stroke: a pilot study combining a gravity-balanced orthosis, functional electrical stimulation, and visual feedback. J Neuro Phys Ther 2009;32:192–202. https://doi.org/10.1097/NPT.0b013e31818e8fc2.
[21] Kirsch NA, Bao X, Alibeji NA, Dicianno BE, Sharma N. Model-based dynamic control allocation in a hybrid neuroprosthesis. IEEE Trans Neural Syst Rehabil Eng 2018;26(1):224–32. https://doi.org/10.1109/TNSRE.2017.2756023.
[22] Durfee W, Palmer K. Estimation of force-activation, force-length, and force-velocity properties in isolated, electrically stimulated muscle. IEEE Trans Biomed Eng 1994;41(3):205–16. https://doi.org/10.1109/10.284939.
[23] Ferrarin M, Pedotti A. The relationship between electrical stimulus and joint torque: a dynamic model. IEEE Trans Rehabil Eng 2000;8(3):342–52. https://doi.org/10.1109/86.867876.
[24] Hussain Z, Tokhi M. Modelling of muscle extension and flexion for FES-assisted indoor rowing exercise. In: 2008 second Asia international conference on modelling & simulation. AMS; 2008. p. 963–7.
[25] Le F, Markovsky I, Freeman CT, Rogers E. Identification of electrically stimulated muscle models of stroke patients. Control Eng Pract 2010;18:396–407. https://doi.org/10.1016/j.conengprac.2009.12.007.
[26] Li Y, Zheng M, Yang Q, Song R. Comparison of two models used to describe the ankle torque in response to functional electrical stimulation. In: 2019 IEEE 4th international conference on advanced robotics and mechatronics; 2019. p. 894–8.
[27] Lim J-K, Nam M-H, Khang G. Model of activation dynamics for an FES-induced muscle fatigue. In: Proceedings of the 22nd annual international conference of the IEEE engineering in medicine and biology society, vol. 3; 2000. p. 2251–3.
[28] Giat Y, Mizrahi J, Levy M. A musculotendon model of the fatigue profiles of paralyzed quadriceps muscle under FES. IEEE Trans Biomed Eng 1993;40(7):664–74. https://doi.org/10.1109/10.237696.
[29] Ding J, Wexler A, Binder-Macleod S. A predictive fatigue model. I. Predicting the effect of stimulation frequency and pattern on fatigue. IEEE Trans Neural Syst Rehabil Eng 2002;10(1):48–58. https://doi.org/10.1109/TNSRE.2002.1021586.
[30] Riener R, Fuhr T. Patient-driven control of FES-supported standing up: a simulation study. IEEE Trans Rehabil Eng 1998;6(2):113–24. https://doi.org/10.1109/86.681177.
[31] Tondu B, Lopez P. Modeling and control of Mckibben artificial muscle robot actuators. IEEE Control Syst Mag 2000;20(2):15–38. https://doi.org/10.1109/37.833638.
[32] Reynolds DB, Repperger DW, Phillips CA, Bandry G. Modeling the dynamic characteristics of pneumatic muscle. Ann Biomed Eng 2003;31(3):310–7. https://doi.org/10.1114/1.1554921.
[33] Slightam JE, Nagurka ML. Robust control law for pneumatic artificial muscles. In: ASME/BATH 2017 symposium on fluid power and motion control; 2017.
[34] Tagami T, Miyazaki T, Kawase T, Kanno T, Kawashima K. Pressure control of a pneumatic artificial muscle including pneumatic circuit model. IEEE Access 2020;8:60526–38. https://doi.org/10.1109/ACCESS.2020.2983602.
[35] Jouppila V, Gadsden A, Ellman A. Modeling and identification of a pneumatic muscle actuator system controlled by on/off solenoid valve. In: Proceedings of the 7th international fluid power conference IFK; 2010. p. 1–34.
[36] Messina A, Giannoccaro NI, Gentile A. Experimenting and modelling the dynamics of pneumatic actuators controlled by the pulse width modulation (pwm) technique. Mechatronics 2005;15(7):859–81. https://doi.org/10.1016/j.mechatronics.2005.01.003.
[37] Bobrow J, McDonell B. Modeling, identification, and control of a pneumatically actuated, force controllable robot. IEEE Trans Robot Autom 1998;14(5):732–42. https://doi.org/10.1109/70.720349.
[38] Rao Z, Bone GM. Nonlinear modeling and control of servo pneumatic actuators. IEEE Trans Control Syst Technol 2008;16(3):562–9. https://doi.org/10.1109/TCST.2007.912127.
[39] Leardini A, O'Connor J, Catani F, Giannini S. A geometric model of the human ankle joint. J Biomech 1999;32(6):585–91. https://doi.org/10.1016/S0021-9290(99)00022-6.
[40] Freeman CT, Hughes AM, Burridge JH, Chappell PH, Lewin PL, Rogers E. A model of the upper extremity using FES for stroke rehabilitation. J Biomed Eng 2009;131(3). https://doi.org/10.1115/1.3005332.
[41] Riener R, Quintern J, Schmidt G. Biomechanical model of the human knee evaluated by neuromuscular stimulation. J Biomech 1996;29(9):1157–67. https://doi.org/10.1016/0021-9290(96)00012-7.
[42] Postans N, Granat M. Effect of functional electrical stimulation, applied during walking, on gait in spastic cerebral palsy. Dev Med Child Neurol 2005;47:46–52. https://doi.org/10.1111/j.1469-8749.2005.tb01039.x.
[43] Malcolm P, Derave W, Galle S, Clercq D. A simple exoskeleton that assists plantarflexion can reduce the metabolic cost of human walking. PLoS ONE 2013;8:e56137. https://doi.org/10.1371/journal.pone.0056137.
[44] Lee H, Rouse E, Krebs H. Summary of human ankle mechanical impedance during walking. IEEE J Trans Eng Health Med 2016;19:2100407. https://doi.org/10.1109/JTEHM.2016.2601613.
[45] Weiss PL, Kearney RE, Hunter IW. Position dependence of ankle joint dynamics–I. Passive mechanics. J Biomech 1986;19(9):727–35. https://doi.org/10.1016/0021-9290(86)90196-x.
[46] Reid MB, Grubwieser GJ, Stokic DS, Koch SM, Leis AA. Development and reversal of fatigue in human tibialis anterior. Muscle Nerve 1993;16(11):1239–45.
[47] Kim SJ, Park J, Shin W, Lee DY, Kim J. Proof-of-concept of a pneumatic ankle foot orthosis powered by a custom compressor for drop foot correction. In: 2020 IEEE international conference on robotics and automation; 2020. p. 747–53.
[48] Kurokawa N, Yamamoto N, Tagawa Y, Yamamoto T, Kuno H. Development of hybrid fes walking assistive system - feasibility study. In: The 2012 international conference on advanced mechatronic systems; 2012. p. 93–7.
[49] Park Y-L, Chen B-r, Pérez-Arancibia NO, Young D, Stirling L, Wood RJ, et al. Design and control of a bio-inspired soft wearable robotic device for ankle foot rehabilitation. Bioinspir Biomim 2014;9:016007. https://doi.org/10.1088/1748-3182/9/1/016007.
[50] Ferris D, Czerniecki J, Hannaford B. An ankle-foot orthosis powered by artificial pneumatic muscles. J Appl Biomech 2005;21:189–97. https://doi.org/10.1123/jab.21.2.189.
[51] Khoobani M, Nazari M, Sepehry N, Ameri M, Sahebi N. A personalized fes-assisted foot drop correction device via a real-time fuzzy controller based on the patient's healthy foot condition. In: 2021 9th RSI international conference on robotics and mechatronics; 2021. p. 497–503.
[52] Copur EH, Freeman CT, Chu B, Laila DS. System identification for FES-based tremor suppression. Eur J Control 2016;27:45–59. https://doi.org/10.1016/j.ejcon.2015.12.003.
[53] Yang K, Meadmore K, Freeman C, Grabham N, Hughes A-M, Wei Y, et al. Development of user-friendly wearable electronic textiles for healthcare applications. Sensors 2018;18(8):1–13.